Modification of RANS Turbulence Models for Pressure Induced Separation on Smooth Surfaces Using the DLR VicToria Experiment

Tobias Knopp
DLR, Institute of Aerodynamics and Flow Technology
Bunsenstraße 10, D-37073 Göttingen
GERMANY

Tobias.Knopp@dlr.de

ABSTRACT

We present a turbulent boundary-layer flow experiment at a significant adverse-pressure gradient with pressure-induced separation on a smooth surface at a high Reynolds number. The experiment was performed by DLR within the internal project VicToria. We describe the design of the test case, the setup in the wind tunnel, and the measurement technique using large-scale particle imaging and Lagrangian particle tracking. We show the experimental results for the mean velocity and for the Reynolds stresses for the evolution of the flow from the zero-pressure gradient region into the adverse pressure gradient region. From the measurement data we motivate wall laws for the mean velocity and for the Reynolds stresses. Then we consider the differential Reynolds stress transport model SSG/LRR-ω. Based on the observation that the length-scale equation is not consistent with the assumed wall laws at adverse-pressure gradient, we propose a modification of the equation for the dissipation rate ω in the model, so that the modified model can predict the proposed wall law at adverse-pressure gradients. Finally we show the numerical results using the modified SSG/LRR-ω model. The modifications cause a reduction of the near-wall flow velocity at adverse-pressure gradients making the modified model more susceptible for flow separation. Both observations are in good agreement with the experimental data.

NOMENCLATURE

Latin symbols

Symbol	Units	Meaning
B_i	1	Coefficient of the log-law at adverse pressure gradient
c_f	1	Skin friction coefficient
c_p	1	Pressure coefficient
H_{12}	1	Shape factor
K_i	1	Slope coefficient of the log-law at adverse pressure gradient
k	m^2/s^2	(Specific) turbulent kinetic energy
P	N/m^2	Mean pressure
R_{ij}	m^2/s^2	Specific Reynolds stress (tensor component)
Re_L	1	Reynolds number based on reference length L

U	m/s	Wall-parallel component of mean velocity
u_τ	m/s	Friction velocity, i.e., velocity scale based on the wall shear stress
u^+	1	Velocity component U scaled to inner viscous units
x	m	Streamwise coordinate, parallel to the floor of the wind-tunnel
y	m	Wall distance
y^+	1	Wall distance in inner viscous units

Greek symbols

Symbol	Units	Meaning
β_k, β_ω	1	Coefficients of the SST k-ω and of the SSG/LRR-ω model, see notation in [24]
γ	1	Coefficient of the production term in the ω-equation, see notation in [24]
δ_{99}	m	Boundary layer thickness based on 99% boundary layer edge velocity criterion
δ*	m	Displacement thickness
θ	m	Momentum loss thickness
κ	1	Coefficient of the slope of the log-law at zero pressure gradient
Δp_x^+	1	Pressure gradient parameter, $\Delta p_x^+ = \nu/(\rho u_\tau^3)\mathrm{d}P/\mathrm{d}x$
ν	m^2/s	Kinematic viscosity of the fluid
ω	1/s	(Specific) rate of turbulent dissipation

Abbreviations

Acronym	Ref.	Meaning
APG		Adverse pressure gradient
CFD		Computational fluid dynamics
DNS		Direct numerical simulation
FPG		Favourable pressure gradient
LES		Large-eddy simulation
LPT		Lagrangian particle tracking
mod κ		Modification of κ at adverse pressure gradient by [13], used in Fig. 8-3 to 8-5

PIV		Particle image velocimetry
PTV		Particle tracking velocimetry
RANS		Reynolds averaged Navier-Stokes equations
RSM		Reynolds stress transport model
STB		Shake the box method
SST *k-ω*	[17]	Two-equation RANS turbulence model by Menter
SSG/LRR*ω*	[19][20]	Differential Reynolds stress model SSG/LRR-ω by Eisfeld
Log-law		Logarithmic law of the wall
Sqrt	[24]	Modification of ω-equation to account for the sqrt-law, used in Fig. 8-3 to 8-5
Sqrt-law	[7][15][24]	Square-root law (or: half-power law)
ZPG		Zero pressure gradient

1.0 INTRODUCTION

The prediction of separation of a turbulent boundary layer on a smooth surface due to an adverse-pressure gradient (APG) in the low-speed regime using RANS-based CFD is still associated with significant uncertainties and open questions. A major hurdle for this is seen in the fact that there is no agreement in the literature on a law of the wall for adverse-pressure gradients. Such a wall law could be used to improve RANS turbulence models similar to the well-known design and calibration of the length-scale equation for the log-law at zero-pressure gradient. In the past decades, there has been a noticeable increase of turbulent boundary layer studies for adverse-pressure gradient since the seminal 1968 conference [1]. Both, experimental studies, e.g., [2], [3] and studies using direct numerical simulations (DNS) were performed, e.g., [4], [5]. However, the number of well-defined and documented validation test cases with a thin separation bubble and at high Reynolds numbers relevant for the flow around aircraft wings are still rare in the literature. The flow features involved in flows with pressure gradient and separation are often even more complex, if surface curvature plays a significant role [6]. For these reasons, a new boundary-layer experiment was designed and performed within the DLR project VicToria. The experiment is based on two earlier experiments conceived by DLR. Regarding these two precursor experiments, the first experiment was performed within the DLR project RETTINA in 2011 and was called RETTINA-I experiment. This experiment was at moderately large Reynolds numbers up to Re_θ=10,000 of the incoming boundary layer before entering the APG region [7]. The second experiment was performed within a common DFG project "Analyse turbulenter Grenzschichten mit Druckgradient bei großen Reynoldszahlen mit hochauflösenden Vielkameramessverfahren" by DLR AS and UniBw Munich (Grant KA 1808/14-1 and SCHR 1165/3-1). It was performed at higher Reynolds numbers up to Re_θ=30,000 of the incoming boundary layer upstream of the APG region, and the adverse-pressure gradient was moderately strong but the flow remained attached and was remote from separation [9]. In the present experiment, the rear part of the geometry was modified to achieve larger adverse-pressure gradients and to cause a thin separation bubble.

Thus the goals of the experiment are (i) to establish a data base for the mean velocity and the Reynolds stresses in the APG region and in the separation region, (ii) to extend a recently proposed wall law at APG (see [24]) towards separation, (iii) to establish the well-defined and documented test case as a validation case for RANS and hybrid RANS/LES methods, and (iv) to extend the recently proposed modification of the *ω*-

equation for the SST k-ω model (see [24]) to the SSG/LRR-ω differential Reynolds-stress model (DRSM) and to calibrate this modification for the situation that the flow approaches separation.

Regarding wall laws at adverse-pressure gradient, the present work will be based on the following ideas published in the literature. The first idea is that there is still a logarithmic region at APG, which becomes smaller as the flow approaches separation, see [11], [12]. Moreover, from the two precursor experiments we found support for the proposal by Nickels in [13] that the log-law slope coefficient decreases at APG with increasing values of the pressure-gradient parameter in inner viscous scaling The next idea is a composite wall law for the inner 15% of the boundary layer by [14]. This composite wall law consists of a log-law in the inner part and a square-root law (abbreviated: sqrt-law) above the log-law in the outer part. In this work we will use the sqrt-law formulation given in [15]. In the two previous experiments [7], [8] , [9] we found support for these hypotheses in the adverse-pressure gradient region sufficiently upstream of the onset of incipient separation. The aim of this experiment is to study this wall law for flows approaching separation.

The status of work on the improvement of RANS models for turbulent boundary layers at adverse-pressure gradient is rare in the literature. One of the few attempts to modify k-ω-type turbulence models for APG was the proposal by Rao and Hassan published in [23]. Their idea was to modify the equation for the turbulent kinetic energy k, so that the modified model gives the sqrt-law for the mean velocity at APG. Therein, Rao and Hassan propose to modify the model for the turbulent diffusion of k by taking into account an additional modeling term which may be associated with the diffusion due to pressure fluctuations and which scales with the streamwise component of the mean pressure gradient. This idea was studied and modified in [24] for the SST k-ω model [17]. Therein the modification of the pressure diffusion term in the k-equation was reduced and a pressure diffusion term was added into the equation for the specific dissipation rate ω. As a second idea presented in [24], the model coefficient of the ω-equation which controls the slope of the log-law was made a function of the pressure-gradient parameter following the idea by Nickels [13]. The underlying idea of both modifications is to make the turbulence model more sensitive to flow separation by reducing the turbulent shear stress in the near wall region by increasing the dissipation of turbulence ε. We base our work on the SSG/LLR-ω model where the length-scale equation is based on ω instead of ε. There is a direct relation between ε and ω and a direct transformation between the ε-equation and the ω-equation, so that the present idea can be applied directly to the ω-equation. In a recent publication [25], the pressure diffusion term was used to modify only the ω-equation for the SSG/LRR-ω model [19][20]. We note that the improvement of RANS models in the inner part of the turbulent boundary layer are expected to improve the predictive accuracy for hybrid RANS/LES methods [18] for flows with separation on a smooth surface.

The impressive improvements in measurement techniques are an additional motivation for wind-tunnel experiments for turbulent boundary layers at adverse-pressure gradient. In the present work we combine particle image velocimetry (PIV) in a large-scale overview measurement setup [7][8][9] and Lagrangian particle tracking velocimetry for the volumetric measurement of all three-components of the mean velocity, which is described, e.g., in [10][26].

The paper is organized as follows: In the first part in sections 2 and 3 we describe the VicToria experiment and the experimental results. Then in sections 4 and 5 we describe a modification for the ω-equation for adverse-pressure gradients for the SSG/LRR-ω model, which was recently proposed in a first version for the SST model in [24]. In section 6 we apply the modified SSG/LRR-ω model to the VicToria experiment. In section 7 we draw the conclusions.

2.0 WIND-TUNNEL EXPERIMENT

The new boundary-layer experiment was designed and performed within the DLR internal project VicToria. The aim was to design a high-Re flow with a slowly increasing adverse-pressure gradient leading to separation from the smooth surface with a thin separation bubble.

2.1 Design of the experiment for RANS model improvement

The major goal of the experiment is to provide a test case and a data base which can be used to improve RANS turbulence models. This leads to the following two aims. The first aim is to establish a data base which provides the data for statistical turbulence modelling. The data are used to study a wall law for the mean velocity at APG, which was recently proposed in [24], but only for moderately strong APG. Thus the aim is to assess and to extend or modify this wall law for strong APG and towards separation using the new experiment. Moreover the experiment is used to assess the strategy to improve RANS turbulence models for APG by using wall laws for the mean velocity and assumptions for the turbulent shear stress at adverse-pressure gradients. A schematic view of the present strategy to improve RANS turbulence models is shown in Figure 8-1.

For the investigation of the wall law, highly resolved data are needed for the mean velocity profile in a thin logarithmic region, which is assumed in a region $80<y^+<150$, and in an assumed square-root law region, which is assumed to be located in a region $300<y^+<0.12\delta_{99}^+$ at strong APG. Moreover, accurate values of the streamwise surface-pressure gradient and of the wall-shear stress are needed.

The additional goal is to identify terms in RANS models whose modelling can be modified so that the model's predictive accuracy for turbulent boundary layers at adverse-pressure gradients can be improved. The data base of 3D3C detail measurements, where all three velocity components are measured in a volumetric field of view using a high-resolution approach, is expected to provide even more detailed data of some terms arising in the transport equation for the Reynolds stresses than the 2D2C standard PIV data, where the two in-plane velocity components in a two-dimensional field of view are measured. However, this depends on current work and progress to improve the 3D3D Lagrangian particle tracking method at DLR [26]. In future research, the data base shall be exploited to identify alternative ideas to improve RSM. For this purpose the aim is to obtain data for the terms of the Reynolds stress transport equation, i.e., the turbulent transport term and the dissipation tensor, which are accessible using the 3D3C Lagrangian particle tracking method.

The test case needs to be at characteristic flow parameters in the region of interest which are relevant for the

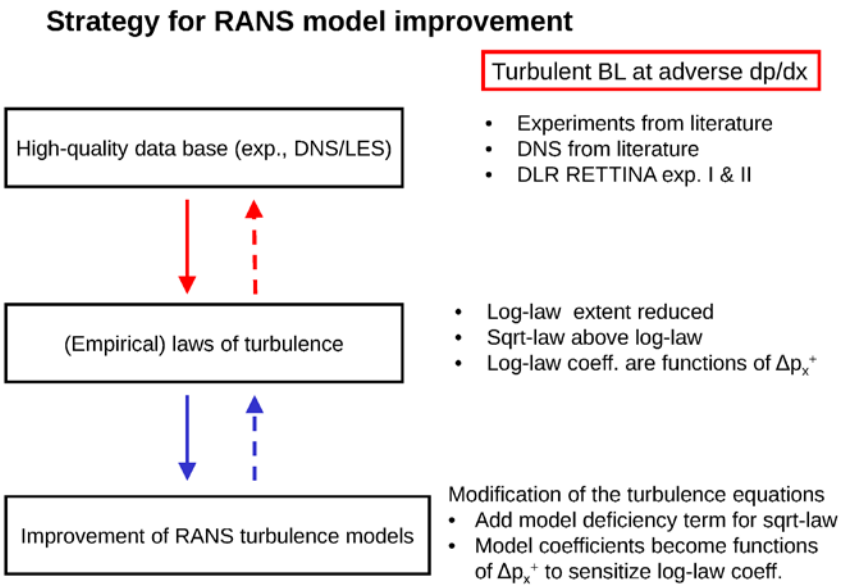

Figure 8-1: Strategy for RANS model improvement for wall bounded flows at adverse pressure gradient with incipient separation.

flow over a wing in high-lift configuration at low-speed for take-off and landing. For this purpose, during the design phase of the experiment we took into account that the characteristic boundary-layer parameters and the pressure gradient in a suitable scaling (i.e., the Rotta-Clauser scaling and in inner viscous scaling) are comparable to the flow over a high-lift wing. The adverse-pressure gradient region and the region of incipient separation are the focus region of the present work.

The other major aim is to establish a well-defined test case with precisely known inflow and outflow conditions. For this reason, special treatment of the boundary layers, e.g., to avoid or reduce undesired early separation on the side walls using blowing or suction, was avoided. At a suitable inlet plane 2D2D PIV data are measured for the mean flow and for the Reynolds stresses, making this test case suitable for RANS and hybrid RANS/LES simulations.

2.2 Experimental setup

We performed the new experiment in the Eiffel-type atmospheric wind tunnel of the University of the German Federal Armed Forces (Universität der Bundeswehr, UniBw) in Munich. The test section is 22 m long and has a cross section of 2 x 2 m^2. The origin of the coordinate system attached to the wind tunnel x = 0 is defined at a position which is located 0.875 m downstream of the smallest diameter of the wind-tunnel nozzle. The contour geometry, often called the test model, is described in Figure 8-2 (left). The flow develops on the wind-tunnel side wall over 4.575 m and is then accelerated along a first ramp of height 0.444 m and of length 1.732 m. Then the flow relaxes over a flat plate of length 4.0 m at almost zero-pressure gradient. Then the flow enters into the region of pressure gradient and surface curvature. The flow follows a first convex deflection of length 0.760 m which initially causes a small FPG, and enters into the APG region. Then there is a second curvilinear deflection of length 0.320 m. The APG focus region is on an inclined flat plate of length 0.762 m at an opening angle of 18.6°.

The geometry was designed with the aid of 2D simulations using the DLR TAU code. For this purpose we used the RANS models by Spalart and Allmaras [16] and the Menter SST model [17], and for some configurations the SSG/LRR-ω model of DLR. The aim of the design study was to obtain flow separation in the rear part of the flat plate. The reason for this is that the Lagrangian particle tracking measurements from behind through the glass plate give the optimal measurement results, since this avoids reflections at the

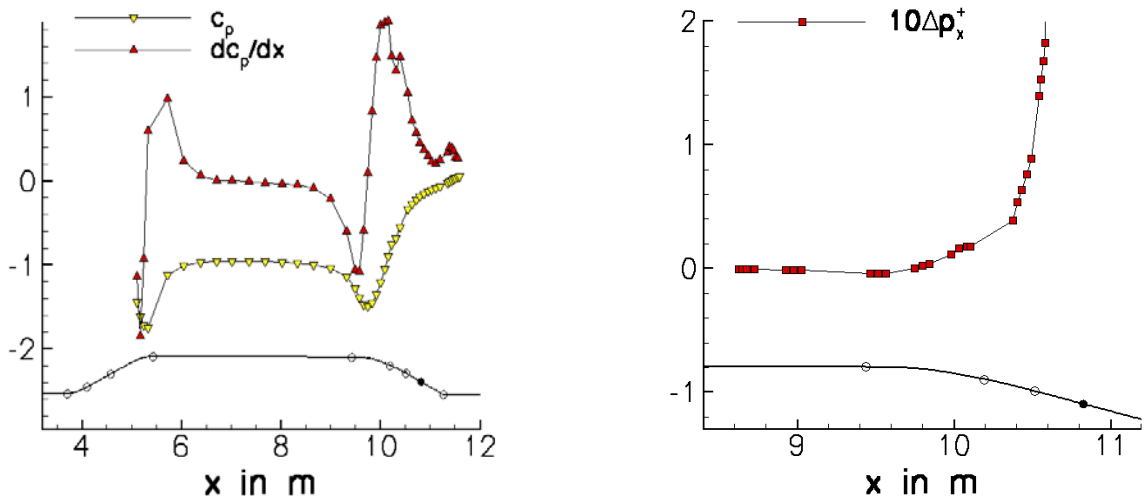

Figure 8-2: Left: Streamwise distribution of c_p and dc_p/dx along the contour of the test model. Right: Streamwise distribution of characteristic pressure gradient parameters in inner viscous scaling Δp_x^+.

aluminium surface of the test model. For this purpose the inclined flat plate has an inset for a glass plate, which enables optical access.

The experiments were performed at different values for the free-stream velocity. As the reference velocity we define the boundary-layer edge velocity above the test model in the ZPG region. The measurements were performed for U_{ref} = 21.07 m/s, 26.61 m/s, 29.25 m/s, and 35.48 m/s. The small divergence angle of the wind-tunnel walls is around 0.13°. The two other wind-tunnel walls are parallel.

2.3 Flow conditions

In the present work we consider the highest Reynolds number case at U_{ref} = 35.48 m/s. The flow conditions and the characteristic boundary-layer parameters are summarized for the reference position at x = 8.629 m in the region of an almost zero-pressure gradient (ZPG) and at the position x = 10.548 m in the adverse-pressure gradient region as the flow approaches separation. This is the position of the 3D3C multi-pulse Lagrangian particle tracking (LPT) measurements. The evaluation of the data is accomplished using the shake-the-box algorithm (STB). The Reynolds number Re_θ based on the momentum thickness θ is 22,600 at the ZPG position and 47,500 at the APG position. The Reynolds number $Re_\tau = u_\tau\ \delta_{99}/\nu$ with the friction velocity u_τ and the 99% boundary-layer thickness δ_{99} is Re_τ=9,300 at the ZPG position and Re_τ=4,600 at the APG position. The pressure-gradient parameter in inner viscous scaling $\Delta p_x^+ = \nu/(\rho u_\tau^3)\mathrm{d}P/\mathrm{d}x$ reaches a high value of Δp_x^+ = 0.163 at the APG position, indicating that the flow is approaching separation, and at this position the pressure-gradient parameter in the Rotta-Clauser scaling reaches a large value of 151. The shape factor H_{12} at this APG position is 1.8.

The distributions for c_p and for $\mathrm{d}c_p/\mathrm{d}x$ are shown in Figure 8-2 (left). The pressure gradient Δp_x^+ in inner scaling is shown in Figure 8-2 (right).

2.4 Measurement technique

The measurements use a combination of different particle imaging approaches. We applied a large-scale overview measurement using a multi-camera 2D2C PIV system with 8 cameras to measure the evolution of the mean velocity from the zero-pressure gradient region to the adverse-pressure gradient region and the region of separation. Each field of view was 0.2 x 0.25 m^2 in streamwise and wall-normal direction and contained the boundary-layer edge. The measurement field was enlarged to 0.2 x 0.3m in the adverse-pressure gradient region, so that the entire boundary layer from the wall up to the outer edge of the boundary layer is measured. The 2D2C PIV data were evaluated using a window correlation method with an interro-gation window size of 16 x 16 px^2. High-resolution data for the Reynolds stresses and for the mean velocity were obtained by using different Lagrangian particle tracking (LPT) approaches together with the shake-the-box (STB) method for the evaluation of the particle tracks from the images. We used the 3D3C LPT STB method in a multi-pulse (MP) acquisition strategy (MP-LPT) [26] and in a time-resolved mode (TR-LPT). The macroscopic field of view was 80 x 90 x 7 mm^3 for the MP-LPT approach.

3.0 EXPERIMENTAL RESULTS

In this section we present the experimental results for the mean velocity for the streamwise evolution of the flow.

3.1 Mean velocity profiles

The mean velocity profiles are made non-dimensional using the so-called inner viscous scaling, i.e., $u^+=U/u_\tau$, $y^+=yu_\tau/\nu$. The friction velocity u_τ is determined by a Clauser chart using all data points in the log-law fit region for the 2D2C PIV data. The y^+-region of the log-law fit was determined for each profile individually.

We observe a region where the mean velocity profile can be fitted by a log-law, see Figure 8-3 (left), even

for large values of Δp_x^+ as the flow approaches separation. We write the log-law in the form

$$u^+ = \frac{1}{K_i}\log(y^+) + B_i \tag{1}$$

Note that we write K_i and B_i instead of κ and B. The observation of a thin log-law region supports the hypothesis of "the resilience of the logarithmic law to pressure gradients" as pointed out by [12]. For each velocity profile, we determine the log-law fit region, i.e., the interval where the mean velocity profile can be fitted by a log-law, by visual inspection. For a moderately strong APG, we find $70 < y^+ < 140$, and for a strong APG we find $20 < y^+ < 80$. The upper edge of this thin region further decreases when approaching separation.

Above the thin log-law fit region, the mean velocity profile can be fitted to a square-root law

$$u^+ = \frac{1}{K_o}\log(y^+) + \frac{1}{2K_o}\left[\sqrt{1+\Delta p_x^+ y^+} - 1 + \log\left(\frac{2}{\sqrt{1+\Delta p_x^+ y^+}+1}\right)\right] + B_o \tag{2}$$

This confirms earlier findings for the two precursor experiments [7][8][9].

The second hypothesis for turbulence modeling part of this work is to assume a significant reduction of the log-law slope coefficient K_i at strong APG. For the present data we can be find indeed a significant reduction of K_i at the position of the strong APG, see Figure 8-3 (left). We found in [7][8][9] that this reduction of the log-law slope coefficient can be described for moderate APG by the model by Nickels [5] which reads

$$K_i = \frac{\kappa_0}{\sqrt{1+\Delta p_x^+ y_c^+}}, \qquad \Delta p_x^+ (y_c^+)^3 + (y_c^+)^2 - Re_c^2 = 0 \tag{3}$$

Therein κ_0=0.39 is the assumed value of the log-law slope for turbulent boundary layers at zero-pressure gradient. Re_c=*12* is an assumed critical value for the stability of the viscous sublayer, which is assumed to be universal for turbulent boundary-layer flows. Finally y_c^+ is the thickness of the viscous sublayer, which is assumed to vary as a function of Δp_x^+, which is described by the second equation in (3).

Regarding the uncertainty of the data, the final evaluation will be subject of future research. The deviation of the wind tunnel velocity between the different measurement campaigns is below 0.5% for the case U=35m/s. The measurement uncertainty for the 2D2C PIV measurement is much smaller than 0.1%, remote from the near wall region, i.e., for y^+>400. For the uncertainty of the skin friction coefficient c_f, the uncertainty of the Clauser chart method to determine the wall shear stress is estimated to be 6% in the zero-pressure gradient region, and around 10% in the region of the moderately strong adverse pressure gradient for Δp_x^+<0.02. For larger values of the pressure gradient parameter, an estimate of the uncertainty cannot be given, since the direct measurement of the wall shear stress using oil film interferometry is still work in progress.

4.0 RANS TURBULENCE MODELING

The starting point for the RANS turbulence modeling is the SSG/LRR-ω model [19][20]. The SSG/LRR-ω was validated for a broad range of aerodynamic flows, see e.g. [21]. This model has demonstrated its maturity for complex industrial configurations in a variety of applications.

4.1 The SSG/LRR-ω model

We write the transport equation for the Reynolds stresses R_{ij} in the form

$$\frac{\partial R_{ij}}{\partial t} + U_k \frac{\partial R_{ij}}{\partial x_k} = P_{ij} - \varepsilon_{ij} + \Pi_{ij} + D^v_{ij} + D^t_{ij} + D^p_{ij} \tag{4}$$

Therein we use the notation that P_{ij} is the production term, ε_{ij} is the dissipation tensor, and Π_{ij} is the pressure-strain correlation tensor. Moreover we introduce the viscous transport term D^v_{ij}, the turbulent transport D^t_{ij} and the transport due to pressure fluctuations D^p_{ij}.

The corresponding transport equation of the turbulent kinetic energy k is

$$\frac{\partial k}{\partial t} + U_j \frac{\partial k}{\partial x_j} = P^k - \varepsilon + D^v + D^t + D^p \tag{5}$$

with production P^k, dissipation ε, and with the corresponding viscous, turbulent and pressure transport terms. The length scale equation in the inner layer is a classical ω-equation

$$\frac{\partial \omega}{\partial t} + U_k \frac{\partial \omega}{\partial x_k} = P_\omega + \varepsilon_\omega + D^v_\omega + D^t_\omega \tag{6}$$

with production term P_ω , dissipation term ε_ω, and with the standard form of the viscous and turbulent contributions to the diffusion of ω, see [27].

4.2 Modification in the inner boundary layer at adverse-pressure gradients

In this section we propose two modifications for the ω-equation for adverse-pressure gradients. The modifications are applied only for the inner 15% of the boundary layer, and the near wall region $y^+<100$ is also excluded. This strategy was presented in [24] for the SST k-ω model. For the mathematical details and for the full notation and nomenclature we refer to [24][25], where we describe the calibration of this modification also for the situation that the flow approaches separation. For a complementary improvement of the SSG/LRR-ω for the flow phenomenon of reattachment we refer to [22].

The first modification is to sensitize the value of the log-law slope coefficient K_i to the pressure-gradient parameter Δp_x^+. For this purpose we use the following relation among the coefficients of the k-ω model, which can be derived for the log-law region at zero-pressure gradient, see [24] [27]

$$\gamma = \frac{\beta_\omega}{\beta_k} - \frac{K_i(\Delta p_x^+)\sigma_\omega}{\sqrt{\beta_k}} \tag{7}$$

Therein γ is the coefficient of the production term P_ω, For the full nomenclature we refer to [24]. Therein $K_i(\Delta p_x^+)$ is given by equation (3). Note that for each field point, the pressure-gradient parameter is given by the value at the corresponding nearest wall point. At adverse-pressure gradient, $K_i(\Delta p_x^+)$ is described by a decreasing function for increasing values of Δp_x^+. Therefore γ takes larger values in a region of a significant adverse-pressure gradient. Then the production term of ω is increased, which increases the values of ω. This causes an increase in the dissipation term in the Reynolds stress equation, i.e., $\varepsilon = \beta_k k\omega$, and in particular in the equation for the turbulent shear stress. This causes then a reduction of the turbulent transport of momentum into the near-wall region. The overall model is then more susceptible for flow separation.

This modification is activated only in the inner 15% of the boundary layer. For this purpose we use a function whose value is one in the inner boundary layer, then decreases for $y>0.15\delta_{99}$ and decays to a value of zero for $y>0.25\delta_{99}$. This function is based on a function by Klebanoff [27]. The intermittency function by Klebanoff describes the decrease of the turbulent viscosity due to the effects of intermittency in the outer part of the boundary layer, see [27]. Moreover we deactivate the modification of γ in the near-wall region $y^+<100$

using a modified van Driest damping function.
The second modification is dedicated to the hypothesis that a square-root law region can be observed for the mean velocity profile. We assume that the square-root law region is located above the log-law region and extends up to 15% of the boundary layer thickness. The modification is motivated by an analysis of the ω-equation using boundary-layer theory. This approach is described in detail in [24][25]. For this purpose we substitute the assumed solution in the sqrt-law region, i.e., the sqrt-law for the mean velocity and a linear relation for the turbulent shear stress. Then we find that the ω-equation is not fulfilled. For this purpose we add a correction term. This term is not only a modification of the value of a coefficient, but alters the functional form. Therefore, the correction term can cause a change of the mean velocity gradient in the sqrt-law region.

The correction term causes an increase of ω in the sqrt-law region. Similar to the first modification described above, this causes an increase in the dissipation term in the Reynolds stress equation, i.e., $\varepsilon = \beta_k k\omega$, and in particular in the equation for the turbulent shear stress. This causes then a reduction of the turbulent transport of momentum towards the wall. This increases the susceptibility of the model for flow separation.

5.0 NUMERICAL SETUP

In this section we describe the setup of the test case for the numerical simulations. We perform two-dimensional simulations of the flow in the mid-span region of the wind tunnel with the contour geometry on the one side and the plain wind tunnel wall on the other side. The wind-tunnel walls have a small divergence angle, given by the experimental setup. We use hybrid meshes generated with the mesh generation tool Centaur. Regarding the mesh resolution, the mesh spacing in streamwise direction is 0.014m in the APG region. The boundary layer is resolved by more than 100 grid nodes. The first node above the wall is at around y^+=1.4 in the zero pressure gradient region at around x=8.6m, which is probably little too large, and y^+<1 in the APG region. The total number of mesh points of the corresponding 2D grid is 220000. The simulations are performed using a special development version of the DLR TAU code. In this version, we use an extended data structure within the code, see [24]. For every wall node we provide a list of field points lying on a wall-normal line. Then surface data like u_τ and Δp_x^+ can be communicated into the field along wall-normal lines. Moreover for each surface point we determine δ_{99}.

6.0 NUMERICAL SIMULATIONS

First we study the results of the simulations in the ZPG region at the streamwise position x = 8.63 m. At this position, the flow has evolved along the flat wall over a streamwise distance of 4 m after the end of the accelerating ramp. The predictions for the SST model and for the SSG/LRR-ω model are close to each other and close to the experimental data, see Figure 8-3 (right). The mean velocity profiles show a good agreement with the experimental data in the logarithmic layer and a reasonably good agreement in the region of the law of the wake, i.e., in the outer part of the boundary layer.

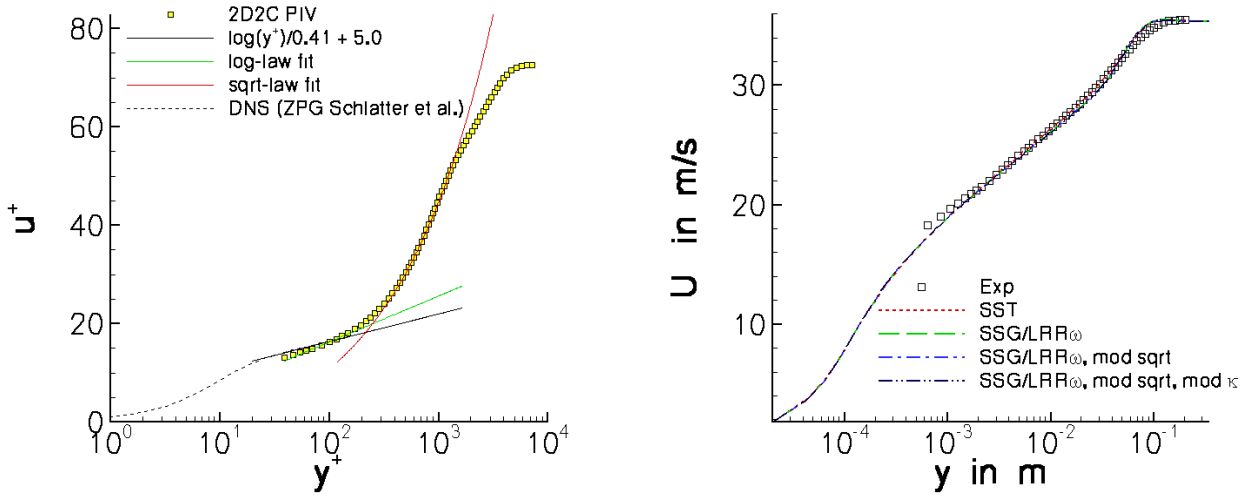

Figure 8-3: Left: Mean velocity profile measured using 2D2C PIV and composite wall-law in the APG region at x=10.55 m. Right: Comparison of RANS simulations and PIV measurement results at x = 8.63 m in the ZPG region.

Then we consider the flow in the APG region. In the APG region at x = 10.407 m, the differences between the SST model and the SSG/LRR-ω model on the one hand and the experimental data on the other hand become larger. The SSG/LRR-ω model predicts a lower mean velocity near the wall for y < 0.01m (or: $y < 0.05\delta_{99}$) than the SST model. However, even the SSG/LRR-ω model overestimates the near-wall flow velocity significantly compared to the experimental data, see Figure 8-4 (left). The same observation can be made for the streamwise position at x = 10.548 m little downstream, see Figure 8-4 (right).

For the modified SSG/LRR-ω model we consider both modifications, i.e., (i) the modification to account for the sqrt-law and (ii) the modification of the coefficient γ which is used to sensitize the log-law slope. First we consider modification (i) alone. This modification causes a reduction of the flow velocity in the near-wall region. For the simulation with modification (i) and (ii) this effect is increased further. Both modifications cause an increase of ω and therefore an increase of the dissipation ε in the equation for the Reynolds stresses. This leads to a reduction of the Reynolds stresses in this region and reduces the transport of wall-parallel momentum towards the wall. Hence the flow becomes more susceptible for separation.

Then we study the predictions for c_f and for the separation point by the RANS models. The results are shown in Figure 8-5. From the PIV data, we infer that the separation point is located at around x = 10.83 m in the mid-span section of the wind-tunnel experiment. First experimental data indicate a spanwise variation of the separation line due to side-wall effects. The standard models predict separation too far downstream, e.g., at x = 10.97m for the SST model. The modified SSG/LRR-ω model improves the predictions. For the modified SSG/LRR-ω model with the sqrt-law modification, the separation point is predicted at x = 10.78m. Using additionally the modification of the log-law slope, the separation point is at x = 10.72m. However, one has to keep in mind that the simulations are two-dimensional. In a three-dimensional simulation the displacement effect of the side-wall boundary layers would be included, which will cause a small but noticeable flow acceleration in the mid-span section. This is expected to shift the separation point further downstream compared to a two-dimensional simulation. The three-dimensional simulations are subject to future work.

7.0 CONCLUSION

In this paper we showed first results of a turbulent boundary-layer flow experiment, where the flow is subjected to an adverse-pressure gradient leading to a thin separation bubble. The flow experiment is well-

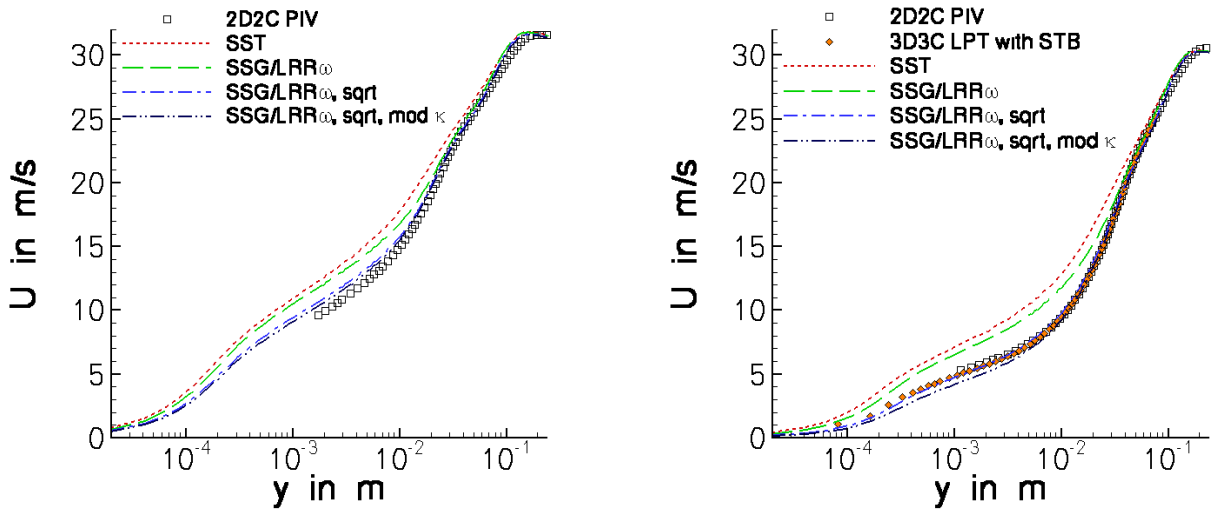

Figure 8-4: Comparison of RANS simulations and PIV measurement results in the APG region at x = 10.41 m (left) and at x=10.55 m. For the estimate of the measurement uncertainties of *U* we refer to section 3.1

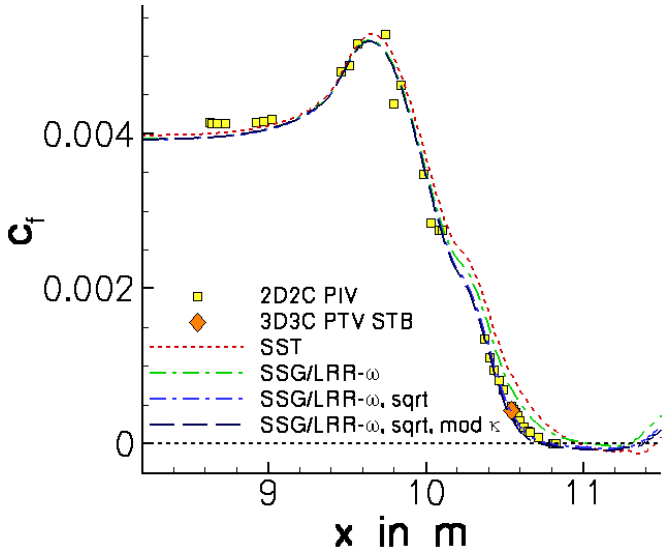

Figure 8-5: Streamwise evolution of the skin friction coefficient and comparison with RANS results. For the estimate of the uncertainties of the experimental data for c_f we refer to section 3.1.

defined so that it is suitable as a validation case for numerical simulations. The measurements confirmed that in the inner part of the boundary layer, the mean velocity profile can be described by a composite wall law with a log-law and a square-root law above the log-law. Based on this hypothesis for the mean velocity profile, we propose a modification of the ω-equation of the SSG/LRR-ω model for adverse-pressure gradient. This modification reduces the dissipation in the inner layer. The modified SSG/LRR-ω model predicts a lower flow velocity in the near-wall region at adverse-pressure gradients and an earlier flow separation. Both are in agreement with the experimental findings. However, the simulations are two-dimensional in the wind-tunnel mid-span section and significant three-dimensional flow effects are expected. In the future work, three-dimensional simulations will be performed. In order to assess the three-dimensionality of the flow, we also performed a visualization of the surface streamlines for quantitative evaluation of the extent of the side-wall separation and the spanwise variation of the separation line.

REFERENCES

[1] Coles, D.E., Hirst, E. A.: Computation of Turbulent Boundary Layers – 1968 AFOSR-IFP-Stanford Conference, Vol II, Stanford University, 1969.

[2] Maciel, Y., Rossignol, K.S., Lemay, J.: A study of a separated turbulent boundary layer in stalled-airfoil-type flow conditions. Experiments in Fluids Vol. 41, pp. 573-590, 2006.

[3] Schatzman, D.M., Thomas, F.O.: An experimental investigation of an unsteady adverse pressure gradient turbulent boundary layer: embedded shear layer scaling. Journal of Fluid Mechanics, Vol. 815, pp. 592-642, 2017.

[4] Manhart, M. and Friedrich, R.: DNS of a turbulent boundary layer with separation. International Journal of Heat and Fluid Flow, Vol. 23, pp. 672–581, 2002.

[5] Coleman, G.N., Rumsey, C.L., Spalart, P.R.: Numerical study of turbulent separation bubbles with varying pressure gradient and Reynolds number. Journal of Fluid Mechanics, Vol. 847, pp. 28-70, 2018.

[6] Baskaran, V., Smits, A. J., Joubert, P.N.: A turbulent flow over a curved hill. Part 1, Growth of an internal boundary layer. Journal of Fluid Mechanics Vol. 182, pp. 47-83, 1987.

[7] Knopp, T., Buchmann, N.A., Schanz, D., Eisfeld, B., Cierpka, C., Hain, R., Schröder, A., Kähler, C. J.: Investigation of scaling laws in a turbulent boundary layer flow at adverse pressure gradient using PIV. Journal of Turbulence, Vol. 16, pp. 250-272, 2015.

[8] Knopp, T. und Buchmann, N.A., Schanz, D., Schröder, A., Cierpka, C., Hain, R. and Kähler, C.J.: Experimental investigation of a turbulent boundary layer subject to an adverse pressure gradient at Re-theta up to 10000 using large-scale and long-range microscopic particle imaging. In: Progress in Wall Turbulence 2 - Understanding and Modeling ERCOFTAC Series, pp. 271-281, 2015.

[9] Knopp, T., Reuther, N., Novara, M., Schülein, E., Schanz, D., Schröder, A., Kähler, C.J.: Investigation of a turbulent boundary layer flow at high Reynolds number using particle-imaging and implications for RANS modeling. In: Proceedings of Tenth International Symposium on Turbulence and Shear Flow Phenomena, July 6-9. 2017, Chicago, USA, 2017.

[10] Schröder, A., Schanz, D., Novara, M., Philipp, F., Geisler, R., Knopp, T., Schroll, M., Willert, C.: Investigation of a high Reynolds number turbulent boundary layer flow with adverse pressure gradients using PIV and 2D- and 3D- Shake-The-Box. In: 19th International Symposium on the Application of Laser and Imaging Techniques to Fluid Mechanics, 16.-19. Jul. 2018, Lisbon, Portugal, 2018.

[11] Dengel, P., Fernholz, H.H.: An experimental investigation of an incompressible turbulent boundary layer in the vicinity of separation. Journal of Fluid Mechanics, Vol. 212, pp. 6155-636, 1990.

[12] Johnstone, R., Coleman, G.N. and Spalart, P.R: The resilience of the logarithmic law to pressure gradients: evidence from direct numerical simulation. Journal of Fluid Mechanics, Vol. 643, pp. 163-175, 2010.

[13] Nickels, T.B.: Inner scaling for wall-bounded flows subject to large pressure gradients. Journal of Fluid Mechanics, Vol. 521, pp. 217–239, 2004.

[14] Perry, A.E., Bell, J.B. and Joubert, P.N.: Velocity and temperature profiles in adverse pressure gradient

turbulent boundary layers I. Journal of Fluid Mechanics, Vol. 25, pp. 299-320, 1966.

[15] Van den Berg, B.: A three-dimensional law of the wall for turbulent shear flows. Journal of Fluid Mechanics, Vol. 70, pp. 149-160, 1975.

[16] Spalart, P.R., Allmaras, S.R.: A one-equation turbulence model for aerodynamic flows, La Recherche Aérospatiale, Vol 1, pp. 5-21, 1994.

[17] Menter, F.R.: Two-Equation Eddy-Viscosity Turbulence Models for Engineering Applications, AIAA Journal, Vol. 32, pp. 1598-1605, 1994.

[18] Spalart, P.R., Deck, S., Shur, M.L., Squires, K.D., Strelets, M. Kh., Travin, A.: A New Version of Detached-eddy Simulation, Resistant to Ambiguous Grid Densities, Theoretical and Computational Fluid Dynamics, Vol. 20, pp.181-195, 2006.

[19] Eisfeld, B., Brodersen, O.: Advanced Turbulence Modeling and Stress Analysis for the DLR-F6 Configuration, AIAA-Paper 2005-4727, 2005.

[20] Cecora, R.-D., Radespiel, R., Eisfeld, B., Probst, A.: Differential Reynolds-Stress Modeling for Aeronautics, AIAA Journal, Vol. 53, pp. 739-755, 2015.

[21] Eisfeld, B., Rumsey, C., Togiti, V.: Verification and Validation of a Second-Moment-Closure Model, AIAA Journal, Vol. 54, pp. 1524-1541, 2016.

[22] Eisfeld, B., Rumsey, C.: Length-Scale Correction for Reynolds Stress Modeling, AIAA-Paper 2019-2961, 2019.

[23] Rao, M.S. and Hassan, H.A.: Modeling turbulence in the presence of adverse pressure gradients. Journal of Aircraft, Vol. 35, pp. 500-502, 1998.

[24] Knopp, T.: A new wall-law for adverse pressure gradient flows and modification of k-ω type RANS turbulence models. AIAA Paper 2016- 0588, 2016.

[25] Knopp, T., Novara, M., Schanz, D., Geisler, R., Philipp, F., Schroll, M., Willert, C., Schröder, A.: Modification of the SSG/LRR-ω RSM for turbulent boundary layers at adverse pressure gradient with separation using the new DLR VicToria experiment. Accepted for publication in: New Results in Numerical and Experimental Fluid Mechanics, Contributions to the 21st STAB/DGLR Symposium Darmstadt, Germany, 2018.

[26] Novara, M., Schanz, D., Reuther, N. , Kähler, C.J. and Schröder, A.: Lagrangian 3D particle tracking in high-speed flows: Shake-The-Box for multi-pulse systems. Experiments in Fluids, Vol. 57, pp. 128 1-20, 2016.

[27] Wilcox, D.C.: Turbulence Modeling for CFD, DCW Industries, La Canada, CA, 3rd Ed., 2006.